Silymarin/curcumin loaded albumin nanoparticles coated by chitosan as muco-inhalable delivery system observing anti-inflammatory and anti COVID-19 characterizations in oleic acid triggered lung injury and *in vitro* COVID-19 experiment

Nemany A.N. Hanafy [*], Maged A. El-Kemary

Nanomedicine group, Institute of Nanoscience and Nanotechnology, Kafrelsheikh University, 33516 Kafrelsheikh, Egypt

ABSTRACT

Respiratory infected by COVID-19 represents a major global health problem at moment even after recovery from virus corona. Since, the lung lesions for infected patients are still sufferings from acute respiratory distress syndrome including alveolar septal edema, pneumonia, hyperplasia, and hyaline membranes Therefore, there is an urgent need to identify additional candidates having ability to overcome inflammatory process and can enhance efficacy in the treatment of COVID-19. The polypenolic extracts were integrated into moeties of bovine serum albumin (BSA) and then were coated by chitosan as a mucoadhesion polymer.

The results of interleukin-6, and c-reactive protein showed significant reduction in group treated by Encap. SIL + CUR (64 ± 0.8 Pg/μL & 6 ± 0.5 μg/μL) compared to group treated by Cham. + CUR (102 ± 0.8 Pg/μL & 7 ± 0.5 μg/μL) respectively and free capsules (with no any drug inside) (148 ± 0.6 Pg/μL & 10 ± 0.6 μg/μL) respectively. Histopathology profile was improved completely. Additionally, encapsulating silymarin showed anti-viral activity *in vitro* COVID-19 experiment. It can be summarized that muco-inhalable delivery system (MIDS) loaded by silymarin can be used to overcome inflammation induced by oleic acid and to overcome COVID-19.

1. Introduction

The acute respiratory distress syndrome (ARDS) is diagnosed as a failure of respiratory system due to accumulate the pulmonary inflammatory cytokines. The progress of this risk leads to increase permeability of endothelial and epithelial cells, formation of pulmonary edema and hypoxemia. Additionally, there have loss of aerated tissue, decrease of lung compliance and bilateral opacities in the chest X-ray image [1]. Histologically, the disruption of alveolar capillary membrane barriers leads to develop noncardiogenic pulmonary edema, in which a proteinaceous exudate floods the alveolar spaces, impairs gas exchange, and precipitates respiratory failure [2]. Although many different types of animal were used as a model to study ARDS including mice [3], rats [4], rabbits [5], guinea pigs [6], dogs [7], sheep [8], pigs [9], horses [10], and nonhuman primates [11]. ARDS continues to be an important global risk particular during infection of coronavirus (COVID-19) that is the main responsible factor to cause and develop ARSD. It is reported that

the pathological examination of lung lesions for patients infected by COVID-19 revealed to presence alveolar septal edema, comprise capillary congestion, desquamation and necrosis of pneumocytes, hyperplasia of alveolar type 2 cells, hyaline membranes, atypical squamous metaplasia, interstitial and intra-alveolar oedema, and thrombi containing platelet-fibrin [12]. The interstitial inflammatory infiltrate consisted mainly of lymphocytes and multinucleated syncytial cell. Since, a spike glycoprotein of COVID 19 can recognize angiotensin converting enzyme 2 (ACE2) facilitating its entry to host cells. These pathological evidences were associated to a severe acute respiratory distress syndrome (SARDS) [13].

For this reason, oleic acid was used here, as a real chemical model can cause strong production of inflammatory process in animal model leading to acute respiratory disorder [14,15]. The pathological feature of this model is similar to that was diagnosed in patients infected by COVID-19 [16]. Since, interleukins (mainly IL-1β and IL-6) can contribute strongly to develop ARDS. On the same way, IL-6 has been

evaluated extensively as a significant indicator for patients infected by COVID-19 [17]. Additionally, c reactive protein (CRP) is an acute phase protein obtained by the liver in response to IL-6 stimulation [18]. It is used as an important indicator for the diagnosis and assessment of severe pulmonary infectious diseases [19]. Previous reports suggested that CRP and IL-6 may also be implicated in the pathophysiology of chronic obstructive pulmonary disease [20]. Thus, CRP level can be used as diagnostic tool in the early stage of COVID-19. Polyphenol and flavonoid compounds such as curcumin and silymarin are identified as natural ligands of peroxisome proliferator-activated receptor-γ, which reduces cytokine production and suppresses the inflammatory process. Therefore, they might play a similar role in protection against lung injury associated with COVID-19 [21]. In this regards, the anti-inflammatory activity of flavonoids and polyphenol compounds have been confirmed strongly [22]. However, the bio-barriers existing in the respiratory airway systems such as mucus, ciliated cells and resident macrophages cause limitation for the localization, penetration and adsorption of drugs in the lung [23].

Our attempt here is to investigate the therapeutic potential effect of encapsulated polyphenolic compounds extracted from chamomile flowers and milk thistle against oleic acid triggered lung injury. Second, is to study the potential therapy of such these compositions against COVID-19. Nanoparticles made of BSA have obtained much interest because of their non-toxicity, their good stability, high drug capacity, and their ability to encapsulate hydrophobic and hydrophilic drugs. BSA NPs coated by second polymer was also investigated by using several polymers such as poly(ethyleneglycol)-modified polyethylenimine, protamine and poly-L-lysine [24]. In the current study, BSA incorporated chitosan was used as ideal carrier for delivering muco inhalable delivery system. Since, chitosan can modify the physiochemical properties of nanoparticles and thus increases the dispersibility of particles leading to increase deposition into the lungs.

2. Material and methods

2.1. Chemicals

Chitosan was purchased from Fluka-Sigma-Aldrich, St. Louis, MO, USA; PBS tablets pH 7.3 was purchased from Oxoid Limited Basingstoke, Hampshire, England; Ethanol from Baker Analyzed, Fisher Scientific, Landsmeer The Netherlands; Bovine serum albumin (BSA); formaldehyde, Dimethyl sulfoxide (DMSO) from Sigma-Aldrich, St. Louis, MO, USA

2.2. Extraction of chamomile flowers and milk thistle

The extract of chamomile flowers and milk thistle were isolated by Hanafy et al. [27] in our bio-nanotechnology lab. Institute of Nanoscience and Nanotechnology, Kafrelsheikh University, Egypt. Briefly, 5 g powder of crushed dry chamomile flowers or milk thistle were kept in a flask containing 100 mL ethanol (96%). The mixture was then stirred for 200 rpm under magnetic stirrer at 70 °C for 2 h. After incubation, the suspension was further filtered through a series of Whatman filters and finally the suspension was passed through 0.22 μm filter. Ethanol was then evaporated and 50 mL distilled water was added. The aqueous solution was lyophilized by freezing dry machine and the extract was stored at −20 °C until use [25].

2.3. High performance liquid chromatography measurement

High performance liquid chromatography (HPLC) was performed by using an Agilent 1260 series. The separation was carried out using Eclipse C18 column (4.6 mm × 250 mm i.d., 5 μm). The mobile phase consisted of water (A) and 0.05% trifluoroacetic acid in acetonitrile (B) at a flow rate 1 mL/min. The mobile phase was programmed consecutively in a linear gradient as follows: 0 min (82% A); 0–5 min (80% A);

5–8 min (60% A); 8–12 min (60% A); 12–15 min (85% A) and 15–16 min (82% A). The multi-wavelength detector was monitored at 280 nm. 10 μL was used as injected volume from each sample. The column temperature was maintained at 35 °C [26].

2.4. Fabrication of MIDS

Extracted chamomile flowers and milk thistle were mixed separately to 50 mL bovine serum albumin (50 mg/100 mL) under magnetic stirrer for 30 min at room temperature. Then, curcumin (5 μg/mL) was added slowly. The mixture was then left under magnetic stirrer for additional 20 min. After that, 20 mL chitosan (50 mg/100 mL) was added and was left for other 20 min under magnetic starrier. Then, the mucoadhesive assembly was dialyzed against distilled water and then was kept at −20 °C for lyophilization [27].

2.5. Determination of loading efficiency

The encapsulation of chamomile flowers and milk thistle extracts were sonicated separately for 15 min with absolute ethanol at 5 amplitude and then they were centrifuged at 14,000 rpm for 40 min. The supernatant was used to calculate the concentration of encapsulated flavonoids by high performance liquid chromatography (HPLC, Agilent Technologies 1200 Infinity series, USA). The HPLC system contains a manual injector (20 μL sample loop) and UV–vis variable wavelength detector with an ultra C18, 5 μm (250 × 4.6 mm, Restek, USA) with detection at 288 nm. Data was processed by Agilent HPLC Chemstation (Rev B.04.03) [28].

2.6. Characterization of MIDS

The characterization of muco-inhalable delivery system was studied by Scanning Electron Microscopy (SEM), Transmission Electron Microscopy (TEM), Fourier Transform Infrared Spectroscopy (FTIR), UV–vis spectroscopy, and Zeta Potential according to [29,30].

2.6.1. Scanning electron microscopy (SEM)
For SEM measurement, few drops of the nanoparticles suspension were dropped onto a template of SEM. after their drying, samples were coated by a 5 nm gold layer and measurements were conducted under 5 kV-accelerating potential electron beam by using SEM (JEOL, JSM–IT 100). Images were processed by using the software SEM/JSM 5000.

2.6.2. Fourier Transform Infrared Spectroscopy (FTIR)
FTIR experiments were carried out by using JASCO Fourier Transform Infrared Spectrometer (JASCO, JAPAN, model no. AUP1200343) to detect the surface molecular structures in the range of 500–4000 cm^{-1} by using KBr pellet method. For all of the measurements, three scans were recorded on different regions on the samples and representative spectra were analyzed.

2.6.3. UV–vis spectrophotometer
The absorbance of inhalable nano aerosolized system was measured by using Jasco V-770 UV Visible Absorbance Spectrophotometer. 500 μL of fabricated micro/nanoparticles was diluted into 4 mL by using distilled water and then scanned at range 200–800 nm.

2.6.4. Zeta potential measurement
The electrophoretic mobility of samples was determined by photon correlation spectroscopy by using a Zeta Nano Sizer. All measurements were performed at 25 °C. Five following measurements were taken for analysis.

2.7. Oleic acid induced lung injury

Oleic acid purchased from Sigma Aldrich company, and then it was

used to induce pulmonary disease [31]. Since, 100 μL oleic acid was diluted by 30% ethanol. The oleate solution was completely sonicated until white turbidity was appeared. Then, it was kept as a stock solution. Afterword, 3 mL of stock solution was diluted to 10 mL saline and used as a working solution. Acute respiratory distress syndrome was induced by inhalable administration for 9 times (3 time exposure/per week). Since, mice were exposed to 5 mL oleate solution each time.

2.8. Animals and ethical approval

25 Male mice were obtained from animal house at TANTA city, Egypt and had weight range of 15–20 g. The mice were housed in polypropylene cages [38 × 23 × 10 cm] with not more than 5 animals per cage and maintained under standard laboratory conditions with natural dark and light cycle. Animal used standard dry rat diet and tap water with free access. Mice were undergone to laboratory conditions one week before beginning of the experiment. All procedures were reviewed and approved by the Animal Ethics Committee controlled by Kafrelsheikh University [25].

2.8.1. Animal model experiment
Mice were subdivided into five groups *i.e.* [n = 5],
G1: Control treated by saline
G2: Oleic acid induced respiratory disease
G3: Oleic acid induced respiratory disease and then they were treated by free capsules
G4: Oleic acid induced respiratory disease, and then they were treated by Encap. Cham. + CUR
G5: Oleic acid induced respiratory disease and then they were treated by Encap. SIL. + CUR.

2.8.2. Blood samples collection.
Blood samples were collected by using anti-coagulant tubes (EDTA) for obtaining blood picture analysis. They were settled by Platelet Count (PLT), Red Blood Cells Count (RBCs), White Blood Cells Count (WBCs), and Haemoglobin concentration (Hb) (mg/dL). While, C-Reactive Protein [32] was measured in serum. Each sample was measured under top serializing and cleaning condition. Sample waste was immediately collected and mixed directly with detergent. All gloves, tubes, musk were collected and wasted.

2.8.3. Photomicrograph acquisition
During dissection of mice, and the examination of lung, photomicrograph for external morphology of lung was obtained.

2.8.4. Histopathology examination
Lungs were removed and fixed by using 10% formalin for 24 h. Then, they were dehydrated by using serial concentrations of ethanol (70%, 80%, 90%, 100%). After word, they were embedded inside paraffin wax after clearing by toluene. The paraffin block was then cut at 5 μm by microtome. The section was stained by H + E and images were further acquired by bright field microscopy.

2.8.5. Interleukin 6 measurement
Enzyme-linked immunosorbent assay was used to detect influence of oleic acid on secretion of inflammatory mediators such as IL-6. Lung was removed from each group and then harvested inside PBS pH 7.2. 100 μL homogenate of each sample was used to quantify the level of IL-6 according to the manufacturer's procedure using Human IL-6 ELISA Kit (Bioassay Technology Laboratory, Shanghai, China). Samples were then measured spectrophotometry at 450 nm. The concentrations were determined by constructing standard curve using recombinant IL-6. The measurement was performed in triplicated [33].

2.8.6. Plaque reduction assay
Plaque inhibition assay for drug susceptibility testing was carried out

in a six multiwells plate with 90% confluent Vero E6 (for SARS-CoV-2 virus) [34]. The treated (Various concentrations in DMEM) and control untreated hCoV-19/Egypt/NRC-03/2020 (Accession Number on GSAID: EPI_ISL_430820) (10-3 dilution of the virus stock) were incubated at room temperature for 1 h. Growth medium was removed from the cell culture plates and the cells were incubated with (100 μL/well) of each virus or virus/compound mixture. After 1 h contact time for virus adsorption, 3 mL of DMEM supplemented with 2% agarose and the tested compounds was added onto the cell monolayer. Then, plates were left to solidify and incubated at 37 °C till formation of viral plaques (3 to 4 days). Formalin (10%) was added for 2 h then plates were stained with 1% crystal violet in distilled water. Control samples were included where untreated virus was incubated with Vero E6 cells and finally plaques were counted and the percent of reduction in plaques formation was recorded as following:

$$\%\text{inhibition} = \text{viral count (untreated)} - \text{viral count (treated)}$$
$$/\text{viral count (untreated)} \times 100$$

2.8.7. Biostatistical analysis
The results were expressed as mean ± standard error of mean (SEM). Data were analyzed by Sigma Plot Software 12.1 using one-way analysis of variance (ANOVA), followed by Duncan's test for comparison between different treatment groups. Statistical significance was set at $P \leq 0.05$.

3. Results

3.1. Flavonoids composition of chamomile flowers and milk thistle extraction

HPLC was used to identify and quantify the encapsulation of flavonoids contents. The concentration of individual flavonoids in the extracts of chamomile flowers and milk thistle was shown in (Fig. 1 and Tables 1 & 2). Since, gallic acid showed good amount in encapsulation (4.96 ± 0.1 μg/mL). While, methyl gallate observed minor amounts (0.03 ± 0.2 μg/mL). The other contents of flavonoids were arranged as following; Gallic acid > Chlorogenic acid > Taxifolin > Caffeic acid > Ellagic acid > Caffeic acid > Naringenin > Ferulic acid > Vanillin > Coumaric acid > Methyl gallate. On the other hand, silymarin content was estimated as (96 ± 0.3 μg/mL).

3.2. Characterization of MIDS

Albumin contains many chemical bonds such as peptide bonds, ionic bonds, hydrogen bonds, covalent bonds, and electrostatic interaction bonds [35] that could facilitate its strong attachment. Such these chemical interactions provide number of advantages allowing to increase stability, bioavailability, high capacity, good storage and control release. In the current study, TEM images showed successful nanoparticles formation. Since, the structure was assembled exactly into 3D structure observing crystals like shape in extract of silymarin (Fig. 2) and semi-spherical or spherical shapes in extract of chamomile flowers (Fig. 3). This behaviour depends mainly on the physical and chemical properties of cargo molecules interacted with used polymers. Confirmly, SEM images showed micro/nanopores were integrated inside moieties of assembly.

In Fig. 4, there is a sharp adsorption at 278 nm in spectrum of BSA that may be attributed to a new transition of the indole moiety of its tryptophan residues when "protonated". Tryptophan residues of proteins are known to participate in π-cation interactions, which are important in protein stability and function [36].

The maximum absorption of chamomile flowers extract was detected at 287 nm according to [37]. In the current study, wide adsorption peak, was detected at spectrum of Encap. (Cham + CUR). This is due to the presence albumin, taxifolin and π-π-curcumin in the same region. While, the characteristic adsorption peak of curcumin was measured at 432 nm
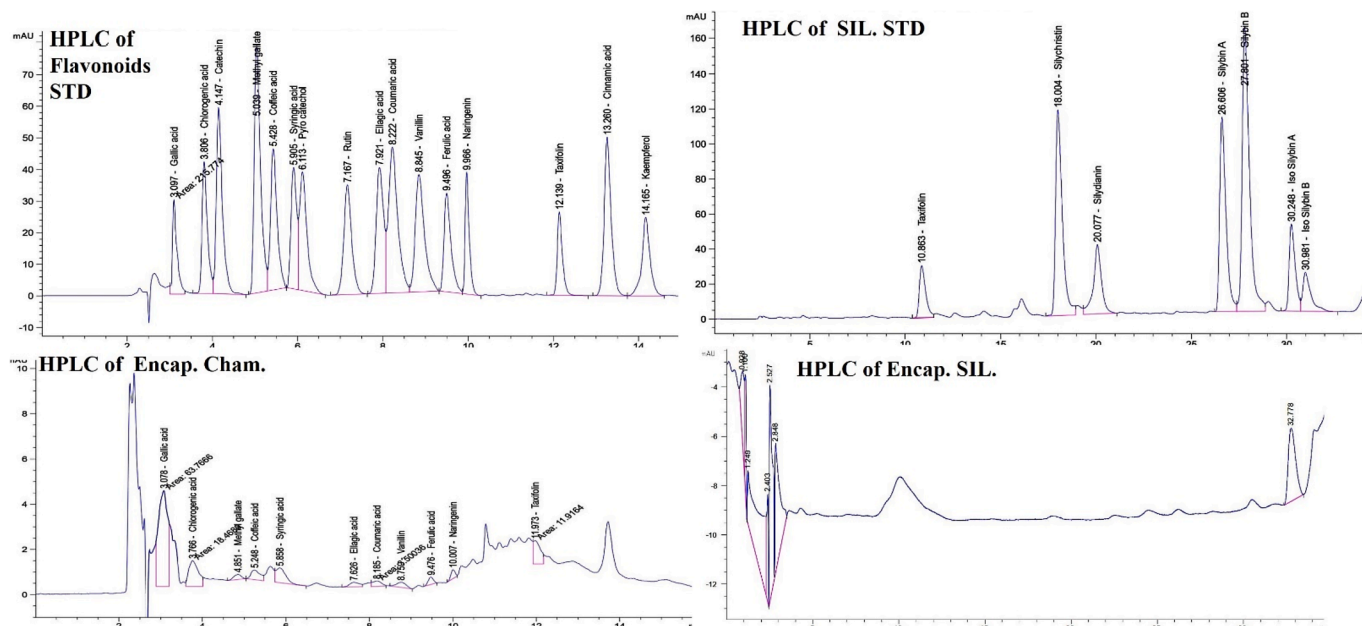
Fig. 1. Chromatography result showed peaks of flavonoids contents isolated after their encapsulation.

Table 1

Quantification and identification of flavonoids contents isolated from chamomile flowers and then were encapsulated.

Flavonoids	Standard flavonoids		Encapsulation of chamomile flowers	
	Area	Conc. (µg/mL)	Area	Conc. (µg/mL)
Gallic acid	215.77	16.8	63.77	4.96 ± 0.1
Chlorogenic acid	366.67	28	18.47	1.41 ± 0.2
Methyl gallate	808.27	10.2	2.75	0.03 ± 0.2
Caffeic acid	482.70	18	6.54	0.24 ± 0.1
Syringic acid	354.12	17.2	10.62	0.52 ± 0.1
Ellagic acid	486.05	34.3	3.26	0.23 ± 0.2
Coumaric acid	701.29	13.2	3.50	0.07 ± 0.1
Vanillin	560.43	12.9	3.60	0.08 ± 0.7
Ferulic acid	356.29	12.4	2.85	0.1 ± 0.3
Naringenin	258.80	15	2.76	0.16 ± 0.2
Taxifolin	219.24	13.2	11.92	0.72 ± 0.4

Table 2

Quantification and identification of flavonoids contents isolated from milk thistle and then were encapsulated.

Flavonoids	Standard		Encapsulation of milk thistle	
	Area	Conc. (µg/mL)	Area	Conc. (µg/mL)
Silymarin	3877	1000	373.4	96 ± 0.3

in both pure curcumin and Encap. (Cham + CUR). While spectrum of Encap. (SIL + CUR) showed three peaks located at (277 nm, 309 nm and 432 nm) that were attributed to (BSA, silymarin and curcumin) respectively. The zeta potential of free mucoadhesive capsules with no any drug inside showed good adsorption (-19 ± 1.5 mV). This reveals presence good physical stability of suspension due to electrostatic repulsion of individual nanoparticles while, zeta potential measurement of Encap. (SIL + CUR) and Encap. (Cham + CUR). was changed into (32 ± 2 mV). Hence, the potential net charge surface was changed into positive charge indicating that polyphenolic extracts can alternate the final charge after their integration into BSA moieties (Fig. 3).

In Fig. 5, FTIR spectrum of BSA alone shows that 3412 cm^{-1} band is assigned to stretching vibration of hydroxyl group whereas 2952 cm^{-1} band was corresponded to stretching vibration of amide I (NH). 1673

cm^{-1} band was related to amide I (mainly C=O stretching vibrations) with a high proportion of α-helix [4]. Band at 1529 cm^{-1} was assigned to amide II [38].

FTIR of chamomile flowers extract showed that band at 3455 cm^{-1} was attributed to OH stretching vibration; band at 2924 cm^{-1}, was associated to stretching vibration of —CH; band at 1644 cm^{-1} was associated with C=O. While band located at 1368 cm^{-1}, was attributed to stretching vibration of —C—O—C.

In the spectrum of curcumin, the adsorption of 3512 cm^{-1} band was associated with phenolic stretching vibration. Additionally, 1644 cm^{-1} and 1515 cm^{-1} bands are attributed to stretching vibration of C=C of benzene rings and olefinic bending vibrations of C—H bound to the benzene rings of curcumin. Stretching vibrations of C—O groups were localized at 811 cm^{-1} [39].

The spectrum of chitosan showed band at 3483 cm^{-1} which was ascribed to the stretching vibration of O—H and N—H. The band at 1630 cm^{-1} was corresponded to the binding vibration of the amido groups. The band in the range 1083 cm^{-1} belongs to the special absorbing peaks of β-1,4 glycoside bond in chitosan [6–7].

In the spectrum of encapsulated chamomile flowers, band at 3383 cm^{-1}, was assigned to stretching vibration of —OH and NH; band at 2924 cm^{-1}, was associated to stretching vibration of —CH; while band located at 1654 cm^{-1}, was assigned to C=O. While, band located at 1083 cm^{-1} belonged to the special absorbed peaks of β-1,4 glycoside bond in chitosan.

While FTIR spectrum of milk thistle extract showed bands at 3412 cm^{-1} associated to phenolic O—H stretching vibration. While, band located at 2927 cm^{-1} was assigned to aromatic C—H stretching vibration. The functional bands of silymarin were located at 1654 cm^{-1} that was attributed to mixed (C=O) amide and (C=C) vibrations, 1403 cm^{-1} band was associated to the symmetric aromatic ring stretching vibration (C=C ring) and 1066 cm^{-1} which was responsible for C—O group.

The spectrum of encapsulating silymarin combined curcumin illustrated that the characteristic bands of silymarin were shifted into 1645 cm^{-1}, 1470 cm^{-1}, and 1079 cm^{-1}.

3.3. Complete blood count (CBC)

The complete blood count showed significant depletion in account of RBCs and haemoglobin compared to control values. While, the platelet
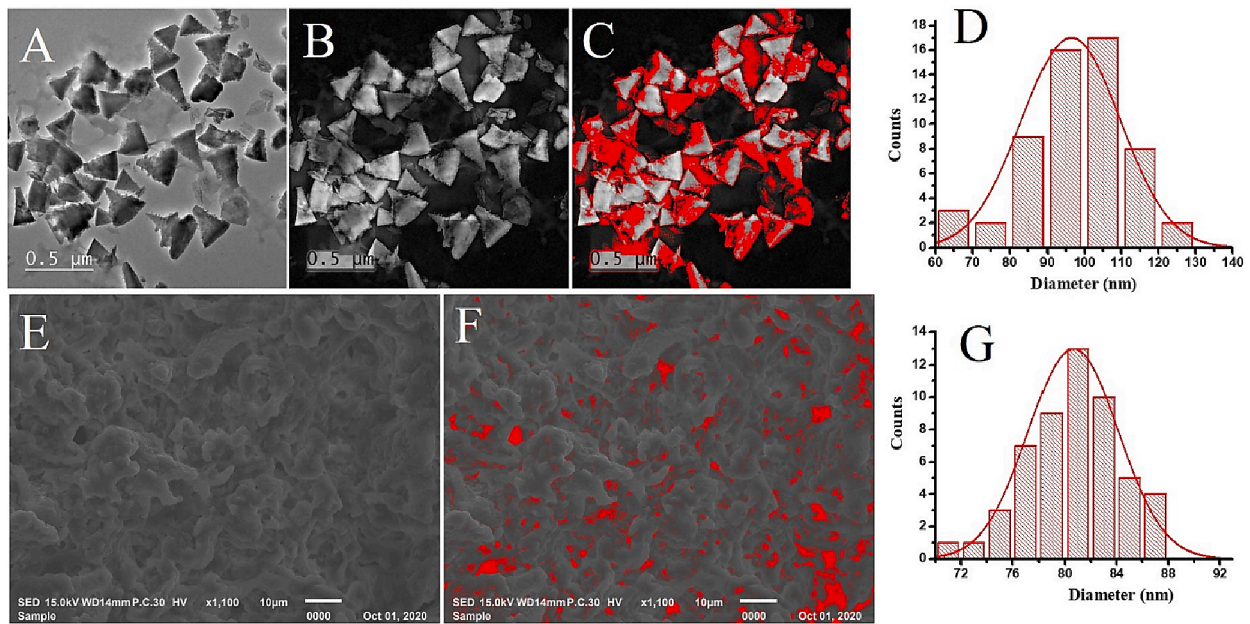
Fig. 2. Morphology of muco-inhaled delivery system. A) TEM image of Encap. (SIL + CUR). B) Grayscale image with invert LUT. C) Graysacle image with thresholding. D) Quantification of distribution diameter of nanoparticles. E) SEM image of Encap. (SIL + CUR). F) Thresholding image. G) Quantification of distribution micro/nanopores.
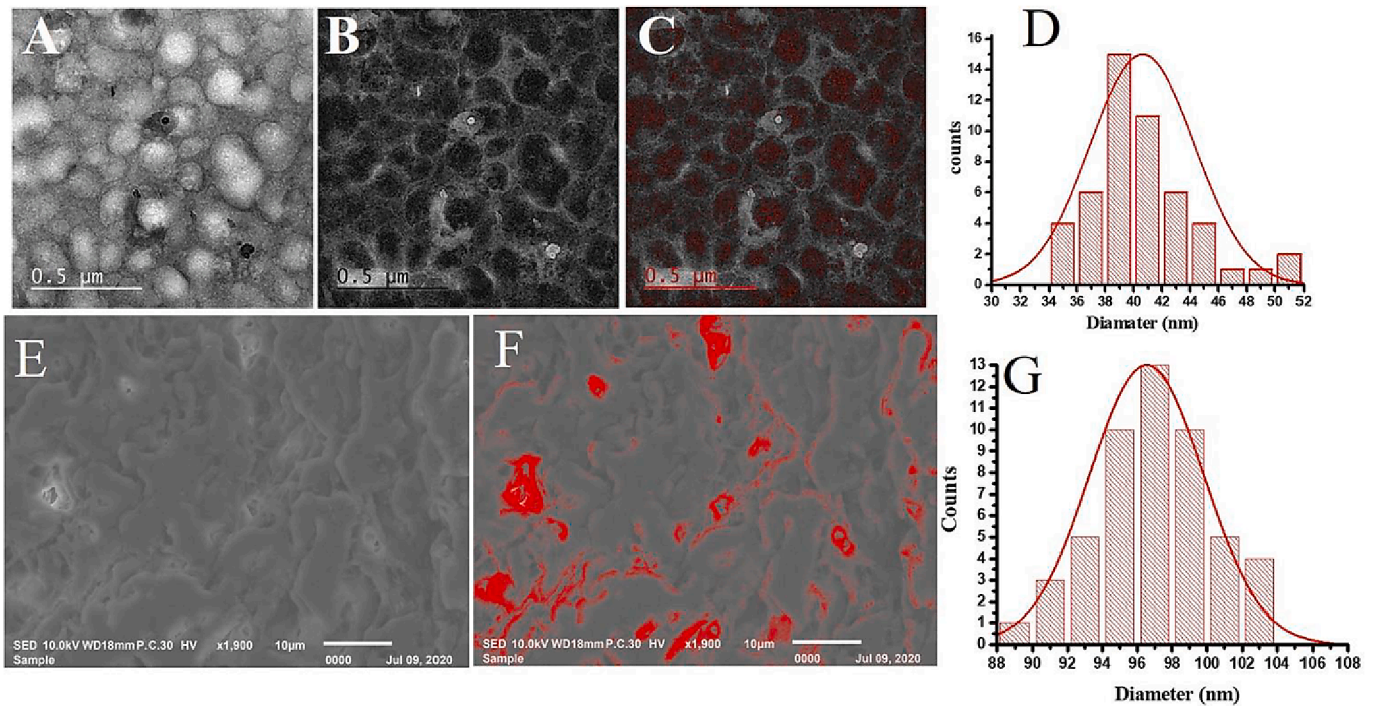
Fig. 3. Morphology of muco-inhaled delivery system. A) TEM image of Encap. (Cham + CUR). B) Grayscale image with invert LUT. C) Graysacle image with thresholding. D) Quantification of distribution diameter of nanoparticles. E) SEM image of Encap. (SIL + CUR). F) Thresholding image. G) Quantification of distribution micro/nanopores.

count was presented higher value in the oleic acid model as shown in Table 3 [40]. In contrast, Encap. SIL + CUR and Encap. Cham. + CUR showed significant improvement of RBCs count, platelets count and haemoglobin level. In meanwhile, oleic acid model treated by free capsules (with no any drug inside) exhibited slightly improvement.

3.4. Photomicrograph results

In the control group, the lungs were appeared as pink colour with very smooth surface and no leakage out of blood was seen under the naked eye. While there is an intense haemorrhage was clearly shown by naked eye in oleic acid model [41] and in group treated by using free capsules (with no any drug inside) compared to control group. Since, oleic acid contains free fatty acid that can react with pulmonary
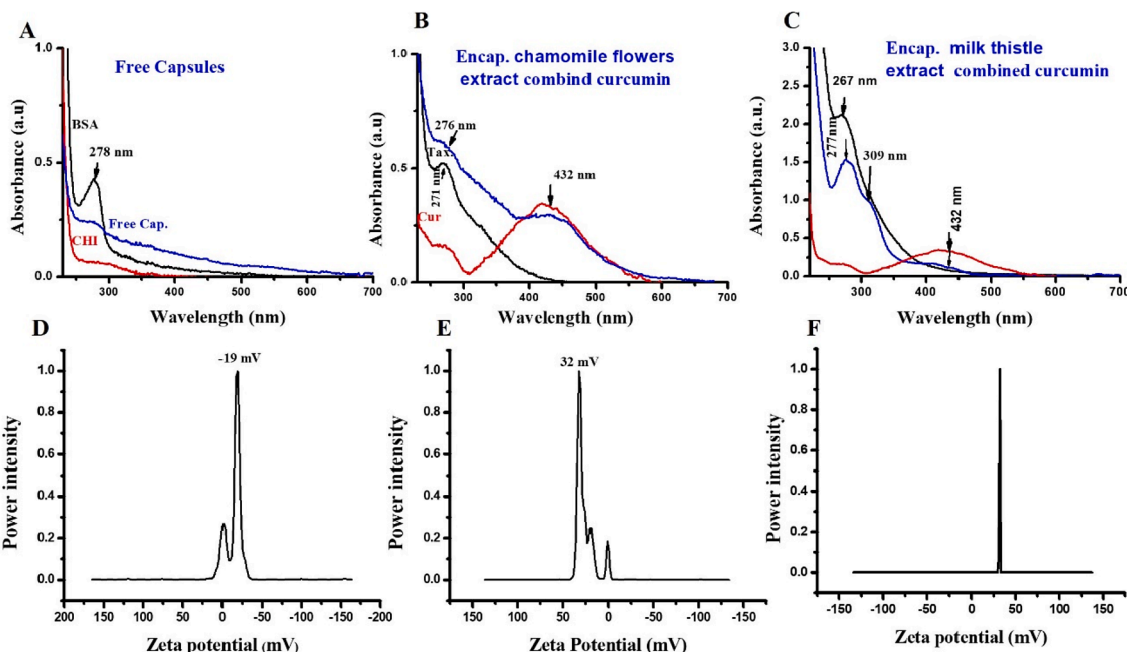
Fig. 4. UV visible spectrophotometer and zeta potential measurements. A & D) Free capsules. B & E) Encap. Cham + CUR. C & F) Encap. SIL + CUR.
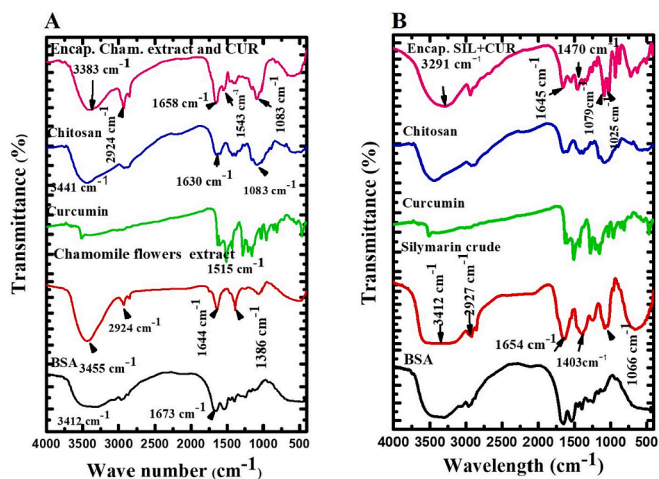
Fig. 5. FTIR measurement for modification bands. A) Encap. Cham. + CUR. B) Encap. SIL + CUR.

Table 3
Complete blood count in different groups.

	Haemoglobin	RBCs	Total leucocytes count	Platelets count
Control	13.3 ± 1.2	9.07 ± 1.1	10.5 ± 1.3	243 ± 2.
Oleic Acid Model	8.7 ± 1.4	6.24 ± 0.8	9.8 ± 1.2	689 ± 3.2
Free Capsules	11.4 ± 0.9	7.8 ± 0.9	11.6 ± 1.2	435 ± 2.5
Encap. SIL + CUR	12 ± 1.3	9.14 ± 1.2	14.8 ± 1.5	380 ± 2.3
Encap. Cham + CUR	10.4 ± 1.2	7.5 ± 0–9	18 ± 1.7	377 ± 1.9

capillary endothelium leading to increase endothelial permeability, inducing pulmonary edema and impairing gas exchange. While, haemorrhage was reduced completely in group treated by encapsulating extracts of milk thistle and chamomile flowers. Previously, haemorrhage was observed in severe ARDS that was diagnosed in patients suffering from complicated leptospirosis (Fig. 5).

3.5. Histopathology results

Alveoli are the functional unit in lung structure, they are mostly coated by alveolar type I and type II cells. Alveolar type I cells contains approximately 90% of the alveolar epithelium, and the remaining 10% is formed by cuboidal type II cells. In the current study, clear alveolar structure and thin alveolar walls, no haemorrhage and no exudate from alveoli were found in the microscopic evaluation. While, the histological changes of oleic acid-induced lung injury were associated with marked functional changes. Since, general polymorphonuclear leukocyte infiltration, along with intra-alveolar edema, haemorrhage, and fibrin deposition. Hyaline membranes, which are depositions of cell debris and plasma proteins lining the alveolar wall, were observed (Fig. 6) [42,43]. In contrast, encapsulated (silymarin and curcumin) was remodulated the histological profile completely and improved histo-architecture of tissue (Fig. 6J & Q).

In the current study, pathological profile of acute lung injury scores was calculated according to previous publication [44]. Since, histopathological examination was investigated as alveolar congestion, alveolar hemorrhages, infiltration or aggregation of neutrophils in the airspace or vessel walls, and thickness of alveolar wall/hyaline membrane formation and inflammatory cell infiltration, were evaluated. The grading scale to score pathologic findings was as follows: 0 = no injury; 1 = slight injury; 2 = moderate injury; 3 = severe injury; and 4 = very severe injury (Fig. 7).

3.6. Interleukin 6 measurement

Interleukin 6 is inflammatory cytokine, used as a clinical examination for measurement of the inflammatory process. Since, IL-6 can be released from monocytes, lymphocytes, or endothelial cells during tissue injury. Therefore, it stimulates neutrophil and platelets from the bone marrow to migrate into blood circulation. IL-6 plays a vital role in an increase expression of c-reactive protein (CRP), fibrinogen, serum amyloid A, and other hemostatic variables. While lipoproteins, and
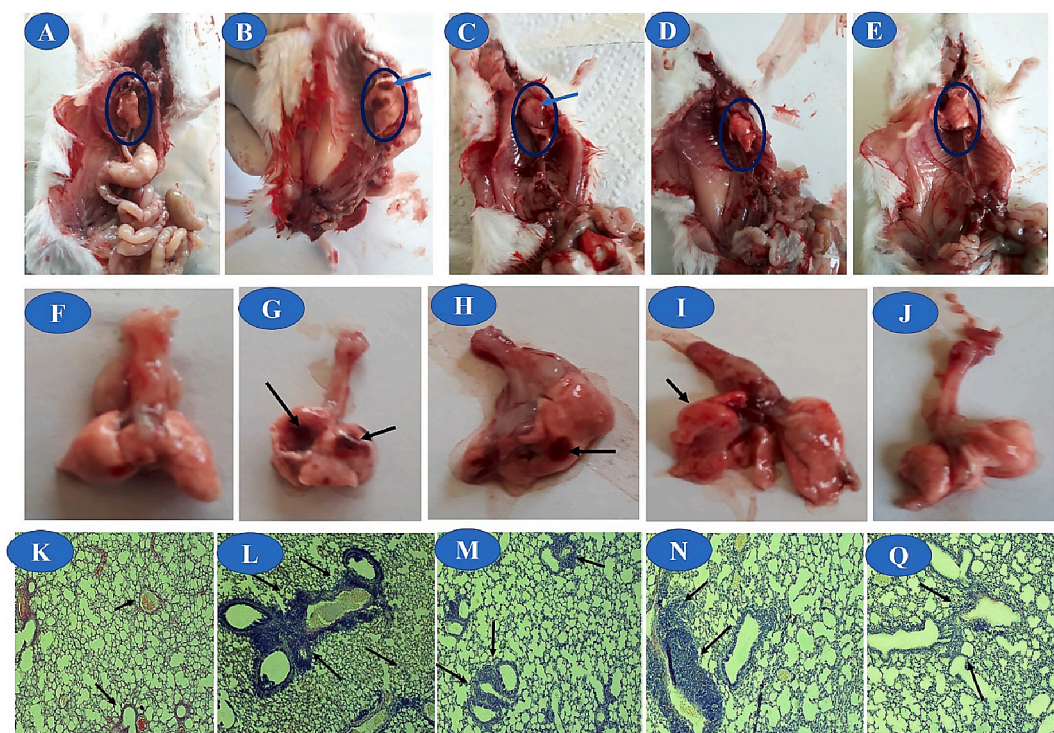
Fig. 6. Photomicrograph of dissecting mice. A) Control. B) Oleic acid model. C) Animal treated by free capsules. D) Animal treated by Encap. Cham. + CUR. E) animal treated by Encap. SIL. + CUR. Photomicrograph of individual lung. F) Control. G) Oleic acid induced model. H) Animal treated by free capsules. I) Animal treated by Encap. Cham. + CUR. J) animal treated by Encap. SIL. + CUR. Histopathological examination K) Control. L) Oleic acid model. M) animal treated by free capsules. N) Animal treated by Encap. Cham. + CUR. Q) Animal treated by Encap. SIL + CUR.
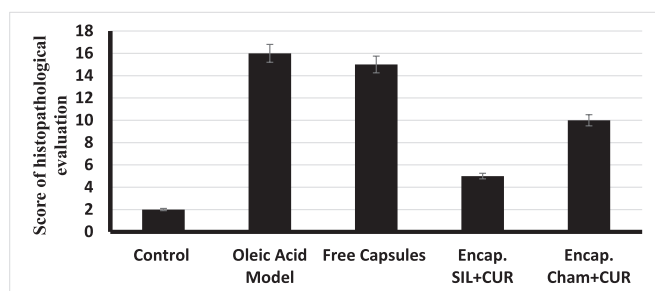
Fig. 7. Scores of histopathological evaluation in different animal groups.

Fig. 8. Evaluation the level of IL-6 (Pg/μL) in different groups showed significant increase in group treated by oleic acid. While there is serious reduction was seen in group treated by encapsulated (silymarin and curcumin).

albumin were decreased during its higher expression [45]. In meanwhile, CRP is a one of the acute phase proteins being synthesized by hepatocytes. The serum concentration of CRP increases during acute stages of diverse diseases associated with inflammation and tissue injury. In the current study, the level of IL-6 was increased significantly in group exposed to oleic acid (175 ± 0.9 Pg/μL). While, its level was reduced significantly in group treated by Encap. SIL + CUR (64 ± 0.8 Pg/μL) compared to group treated by Cham. + CUR (102 ± 0.8 Pg/μL) and free capsules (with no any drug inside) (148 ± 0.6 Pg/μL) (Fig. 8). Similarly, Encap. SIL + CUR has ability to reduce completely CRP level in group treated by oleic acid (6 ± 0.5 μg/μL). While, the level of CRP was reduced slightly in group treated by Encap. Cham. + CUR (7 ± 0.5 μg/μL) compared to oleic acid model (12 ± 0.8 μg/μL) and group treated by free capsules alone (10 ± 0.6 μg/μL) (Fig. 9).

3.7. Plaque reduction assay

Plaque-based assay is a standard technique used to determine virus concentration in terms of infectious dose [46]. Viral plaque assays determine the number of plaque forming units (pfu) in a virus sample, which is one measure of virus quantity. A confluent monolayer of host cells was infected by COVID-19 and the infected cell area created a plaque (an area of infection surrounded by uninfected cells) which can be seen with an optical microscope. In plaque reduction assay, Encap. (SIL. + CUR) nanoparticles were added in different concentrations (3.125, 6.25, 12.5 and 25 μg/mL) to infected cells and numbers of formed plaques were counted and compared to controls (untreated infected cells). Finally, percent of the reduction in plaques formation in comparison to control was recorded. In Table 4 and Fig. 10, the Encap. (SIL. + CUR) showed antiviral activity 44.4% against SARS-CoV-2 at the
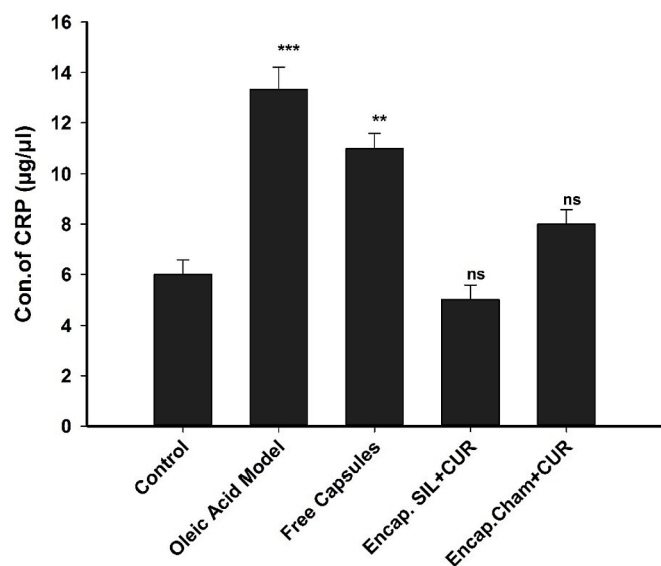
Fig. 9. Evaluation the level of CRP (µg/µL) in different groups showed significant increase in group treated by oleic acid. While there is serious reduction was seen in group treated by encapsulated (silymarin and curcumin).

Table 4
Antiviral activity against Severe Acute Respiratory Syndrome Coronavirus 2 (SARS-CoV2) as measured by plaque reduction assay.

Code of sample	Conc. (µg/mL)	Virus control (PFU/mL)	Viral titer post-treatment (PFU/mL)	Viral inhibition (%)
Number 1	25	2.7 * 10^6	1.5 * 10^6	44.4%
	12.5		1.55 * 10^6	42.6%
	6.25		1.85 * 10^6	31.5%
	3.125		2.05 * 10^6	24.1%
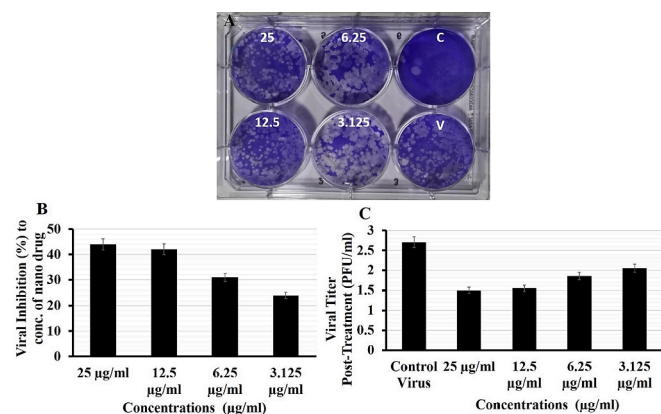
Fig. 10. Plaque reduction assay. A) Plate of plague reduction. B) Quantification of viral inhibition (%). C) Quantification of viral titer post treatment.

highest tested concentration (25 µg/mL) and this inhibition was decreased gradually to 24.1% at the lowest tested concentration (3.125 µg/mL).

4. Discussion

Nanoparticles made of chitosan have been strongly introduced for pulmonary administration due to its mucoadhesive properties. Chitosan contains many amino groups (—NH2) that can be protonated (—NH3 +) at acidic pH. Such this cationic charge of chitosan enables delivery to

adhere and penetrate the mucosa of lung epithelial cells. This facilitates cellular internalization and drug accumulation. Since mucoadhesive polymer can help to open the intercellular tight junctions of the lung epithelium [4]. In meanwhile, BSA contains lysine and glutamate that make it suitable carrier to carry high amount of incorporated flavonoids inside its moieties [47].

In the current study, chitosan-BSA NPs loaded separately by extracts of chamomile flowers and milk thistle were mostly assembled into 3D network structure with many micro/nanopores. SEM images showed exactly presence several pores integrated into chitosan-BSA moieties and distributed inside the surface (Figs. 2 & 3). Zeta potential and UV visible spectrophotometer measurements confirmed the successful incorporation of assembly. Since, chitosan-BSA NPs obtained (-19 ± 1.5 mV). While, the encapsulation of curcumin with extracts of chamomile flowers and milk thistle showed (32 ± 2 mV). The main absorbance peak of curcumin was observed at 432 nm indicating to presence of curcumin in both assemblies. In the current study, FTIR was used to study the modification of chemical bands after their reaction. Chitosan, BSA, curcumin, extract of chamomile flowers, milk thistle and the nano formulation were investigated. The spectrum of encapsulating milk thistle extract (silymarin) combined curcumin illustrated that the characteristic bands of silymarin were shifted into 1645 cm^{-1}, 1470 cm^{-1}, and 1079 cm^{-1}. While, extract of chamomile flowers combined curcumin showed shifting peak of 1644 cm^{-1} to 1654 cm^{-1} (Fig. 5).

FTIR result indicates that extract of chamomile flowers and milk thistle were successfully incorporated inside moieties of assembly. To confirm this result, chromatography analysis of encapsulated flavonoids showed that concentration of flavonoids content were arranged as following; Gallic acid > Chlorogenic acid > Taxifolin > Caffeic acid > Ellagic acid > Caffeic acid > Naringenin > Ferulic acid > Vanillin > Coumaric acid > Methyl gallate (Fig. 1). Recently, many reports have confirmed possible induction of ARDS with similar pathological evidence in animal model by using oleic acid [48]. Since, oleic acid causes accumulation of neutrophil, increase in the level TNF, IL-8, IL-6 and IL-1β. This leads to loss of the alveolar-capillary barrier and forms the hyaline membrane formation [49]. In the current study, oleic acid animal model was developed as an attempt to study ARDS. The presented DATA showed significant increase in IL-6 and CRP as cytokines indicator for acute inflammation (oleic acid model). In contrast, the level of IL-6 was reduced significantly in group treated by Encap. (SIL. + CUR) (64 ± 0.8 Pg/µL) compared to Encap. (Cham. + CUR) (102 ± 0.8 Pg/µL). Similarly, CRP level was exactly inhibited in oleic acid model treated by Encap. (SIL. + CUR) (6 ± 0.5 µg/µL). compared to group treated by Encap. (Cham. + CUR) (7 ± 0.5 µg/µL). Besides that, silymarin NPs exhibited antiviral activity against COVID-19 at concentration 25 µg/mL (Fig. 10 and Table 4). This result indicates that silymarin NPs have strong potential therapy against acute inflammation. Hence, they can improve histopathological evidence. Additionally, they have ability to reduce growth of COVID-19.

It can be summarized that silymarin extracted from milk thistle, has a protective effect during lung injury because of its ability to decrease the production of nitric oxide, decrease the infiltration of inflammatory cells, suppress the activity of myeloperoxidase and its ability to reduce the protein levels of pro-inflammatory mediators, superoxide dismutase, catalase and GSH peroxidase [50]. Additionally, silymarin has been considered recently as a potent inhibitor for angiotensin converting enzyme-2 preventing its host-cell entry [51].

Chamomile has been used extensively as anti-microbial, anti-inflammatory, anti-spasmic, analgesic and sedative properties. This is because of its content from biological active compounds including essential oils and several polyphenols. Recently, chamomile extract has been considered as a good candidate, can be used for the treatment of respiratory symptoms especially when used as nasal irrigation because of its ability to reduce leukocyte infiltration, providing anti-inflammatory behaviour. According to this fact, chamomile extract has been used recently as a promising treatment for Covid-19 [52,53].

Similarly, curcumin represents a natural ligand can bind to peroxisome proliferator-activated receptor-γ, which represses the inflammatory process by reducing cytokine production [54]. On the same way, many reports have revealed the ability of curcumin to bind with Mpro protease, indispensable for the maturation of SARS-CoV-2 [55]. Therefore, it can bind to the glycoprotein receptor-binding domain and to the peptidase –ACE2 domain, which are necessary for the entry of the virus [56]. For this reason, our hypothesis was assessed to integrate curcumin with extract of chamomile flowers and milk thistle separately to raise the potential activity of total polyphenolic extract in treatment of inflammatory mediators and to have potential therapy against lung injury associated with COVID-19 [57,58].

5. Conclusion

Many antivirus drugs have been derived recently into clinical trial. However, less of them may provide clear improvement for lung pathological profiles during treatment. In the current study, oleic acid model showed polymorphonuclear leukocyte infiltration, along with intra-alveolar edema, haemorrhage, and fibrin deposition. Hyaline membranes. This pathological profile was significantly remodulated by encapsulated silymarin + curcumin. In meanwell, IL-6 and CRP were significantly reduced in oleic acid model as well after their treatment. Additionally, encapsulated silymarin + curcumin exhibited antiviral activity against COVID19 by using plague reduction assay. Nanotechnology have been used widely in biomedical application to overcome drawbacks of pure drugs [59–62].

CRediT authorship contribution statement

N.A.N. H. designed, wrote, supervised the manuscript; M. A. E. revised and supervised the manuscript. All authors read and approved the final review version.

Declaration of competing interest

Authors declare that there is no any conflict of interest.

References

[1] J.A. Lorente, A. Ballén-Barragán, R. Herrero, A. Esteban, Acute respiratory distress syndrome: does histology matter? Crit. Care 19 (1) (2015) 337, https://doi.org/10.1186/s13054-015-1022. Published 2015 Sep 15.

[2] J.N. Gonzales, R. Lucas, A.D. Verin, The acute respiratory distress syndrome: mechanisms and perspective therapeutic approaches, Austin J. Vasc. Med. 2 (1) (2015) 1009.

[3] H. Gong, J. Rehman, H. Tang, K. Wary, P. Chatturvedi, Y. Zhao, Y. A. Komorova, S.M. Vogel, A.B. Malik, HIF2α signaling inhibits adherens junctional disruption in acute lung injury, J. Clin. Invest. 125 (2015) 652–664.

[4] Y. Xin, G. Song, M. Cereda, S. Kadlecek, H. Hamedani, Y. Jiang, J. Rajaei, J. Clapp, H. Profka, N. Meeder, J. Wu, N.J. Tustison, J.C. Gee, R.R. Rizi, Semiautomatic segmentation of longitudinal computed tomography images in a rat model of lung injury by surfactant depletion, J. Appl. Physiol. 118 (2015) 377–385.

[5] F.J. Walther, J.M. Hernandez-Juviel, L.M. Gordon, A.J. Waring, Synthetic surfactant containing SP-B and SP-C mimics is superior to single-peptide formulations in rabbits with chemical acute lung injury, Peer J 2 (2014), e393.

[6] S.M. Kabir, S. Mukherjee, V. Rajaratnam, M.G. Smith, S.K. Das, Desensitization of beta-adrenergic receptors in lung injury induced by 2-chloroethyl ethyl sulfide, a mustard analog, J. Biochem. Mol. Toxicol. 23 (2009) 59–70.

[7] Y. Yang, Q. Chen, S. Liu, Y. Huang, L. Liu, X. Wu, G. Chen, J. Jin, G. Teng, H. Qiu, Effects of recruitment maneuvers with PEEP on lung volume distribution in canine models of direct and indirect lung injury, Mol. Biol. Rep. 41 (2014) 1325–1333.

[8] S. Asmussen, H. Ito, D.L. Traber, J.W. Lee, R.A. Cox, H.K. Hawkins, D.F. McAuley, D.H. McKenna, L.D. Traber, H. Zhuo, J. Wilson, D.N. Herndon, D.S. Prough, K. D. Liu, M.A. Matthay, P. Enkhbaatar, Human mesenchymal stem cells reduce the severity of acute lung injury in a sheep model of bacterial pneumonia, Thorax 69 (2014) 819–825.

[9] A. Ziebart, E.K. Hartmann, R. Thomas, T. Liu, B. Duenges, A. Schad, M. Bodenstein, S.C. Thal, M. David, Low tidal volume pressure support versus controlled ventilation in early experimental sepsis in pigs, Respir. Res. 15 (2014) 101.

[10] N. Fard, A. Saffari, G. Emami, S. Hofer, H.U. Kauczor, A. Mehrabi, Acute respiratory distress syndrome induction by pulmonary ischemia-reperfusion injury in large animal models, J. Surg. Res. 189 (2014) 274–284.

[11] R.R. Hukkanen, H.D. Liggitt, R.D. Murnane, C.W. Frevert, Systemic inflammatory response syndrome in nonhuman primates culminating in multiple organ failure, acute lung injury, and disseminated intravascular coagulation, Toxicol. Pathol. 37 (2009) 799–804.

[12] L. Carsana, A. Sonzogni, A. Nasr, et al., Pulmonary post-mortem findings in a series of COVID-19 cases from northern Italy: a two-centre descriptive study, Lancet Infect. Dis. 20 (10) (2020) 1135–1140, https://doi.org/10.1016/S1473-3099(20)30434-5.

[13] M.Y. Liu, B. Zheng, Y. Zhang, J.P. Li, Role and mechanism of angiotensin-converting enzyme 2 in acute lung injury in coronavirus disease 2019, Chronic Dis. Transl. Med. 6 (2) (2020 Jun) 98–105.

[14] C.F. Gonçalves-de-Albuquerque, A.R. Silva, P. Burth, M.V. Castro-Faria, H. C. Castro-Faria-Neto, Acute respiratory distress syndrome: role of oleic acid-triggered lung injury and inflammation, Mediat. Inflamm. 2015 (2015), 260465.

[15] S. Hülsmann, S. Khabbazzadeh, K. Meissner, M. Quintel, A potential role of the renin-angiotensin-system for disturbances of respiratory chemosensitivity in acute respiratory distress syndrome and severe acute respiratory syndrome, Front. Physiol. 20 (11) (2021 Jan), 588248.

[16] X. Zhang, S. Li, S. Niu, ACE2 and COVID-19 and the resulting ARDS, Postgrad. Med. J. 96 (1137) (2020 Jul) 403–407.

[17] S. Tyagi, P. Gupta, A.S. Saini, C. Kaushal, S. Sharma, The peroxisome proliferator-activated receptor: a family of nuclear receptors role in various diseases, J. Adv. Pharm. Technol. Res. 2 (4) (2011) 236–240, https://doi.org/10.4103/2231-4040.90879.

[18] M.B. Pepys, G.M. Hirschfield, G.A. Tennent, J.R. Gallimore, M.C. Kahan, V. Bellotti, Targeting C-reactive protein for the treatment of cardiovascular disease.A critical update, J. Clin. Invest. 111 (2003) 1805–1812.

[19] S. Chalmers, A. Khawaja, P.M. Wieruszewski, O. Gajic, Y. Odeyemi, Diagnosis and treatment of acute pulmonary inflammation in critically ill patients: the role of inflammatory biomarkers, World J. Crit. Care Med. 8 (5) (2019) 5971, https://doi.org/10.5492/wjccm.v8.i5.59.

[20] H. Matsumoto, T. Kasai, A. Sato, S. Ishiwata, S. Yatsu, J. Shitara, et al., Association between C-reactive protein levels at hospital admission and long-term mortality in patients with acute decompensated heart failure, Heart Vessel. 34 (12) (2019) 1961–1968, https://doi.org/10.1007/s00380-019-01435-9.

[21] H. Gupta, M. Gupta, S. Bhargava, Potential use of turmeric in COVID-19, Clin. Exp. Dermatol. 45 (7) (2020) 902–903, https://doi.org/10.1111/ced.14357.

[22] N. Leyva-López, E.P. Gutierrez-Grijalva, D.L. Ambriz-Perez, J.B. Heredia, Flavonoids as cytokine modulators: a possible therapy for inflammation-related diseases, Int. J. Mol. Sci. 17 (6) (2016) 921.

[23] M. Karimi, P. Avci, R. Mobasseri, M.R. Hamblin, H. Naderi-Manesh, The novel albumin-chitosan core-shell nanoparticles for gene delivery: preparation, optimization and cell uptake investigation, J. Nanopart. Res. 15 (4) (2013) 1651, https://doi.org/10.1007/s11051-013-1651.

[24] J.K. Srivastava, S. Gupta, Extraction, characterization, stability and biological activity of flavonoids isolated from chamomile flowers, Mol. Cell. Pharmacol. 1 (3) (2009 Jan 1) 138.

[27] L.W. Chang, M.L. Hou, T.H. Tsai, Silymarin in liposomes and ethosomes: pharmacokinetics and tissue distribution in free-moving rats by high-performance liquid chromatography-tandem mass spectrometry, J. Agric. Food Chem. 62 (48) (2014 Dec 3) 11657–11665.

[25] N.A.N. Hanafy, Starch based hydrogel NPs loaded by anthocyanins might treat glycogen storage at cardiomyopathy in animal fibrotic model, Int. J. Biol. Macromol. 183 (2021) 171–181.

[26] N.A.N. Hanafy, M. El-Kemary, S. Leporatti, Mucoadhesive curcumin crosslinked carboxy methyl cellulose might increase inhibitory efficiency for liver cancer treatment, Mater.Sci.Eng.C (2020), 111119.

[28] N.A.N. Hanafy, S. Leporatti, M.A. El-Kemary, Extraction of chlorophyll and carotenoids loaded into chitosan as potential targeted therapy and bio imaging agents for breast carcinoma, Int. J. Biol. Macromol. 182 (2021) 1150–1160.

[29] M.J. Ohrabi, A.R. Dehpour, F. Attar, A. Hasan, N. Mohammad-Sadeghi, A. A. Meratan, F.M. Aziz, A. Salihi, M.S. Shekha, K. Akhtari, K. Shahpasand, S.M. M. Hojjati, M. Sharifi, A.A. Saboury, S.M. Rezayat, S.E. Mousavi, M. Falahati, Silymarin-albumin nanoplex: preparation and its potential application as an antioxidant in nervous system in vitro and in vivo, Int. J. Pharm. 15 (572) (2019 Dec), 118824.

[30] N.A.N. Hanafy, I. Fabregat, S. Leporatti, M.E. Kemary, Encapsulating TGF-β1 inhibitory peptides P17 and P144 as a promising strategy to facilitate their dissolution and to improve their functionalization, Pharmaceutics 12 (2020) 421.

[31] N.A.N. Hanafy, Optimally designed theranostic system based folic acids and chitosan as a promising mucoadhesive delivery system for encapsulating curcumin LbL nano-template against invasiveness of breast cancer, Int. J. Biol. Macromol. 182 (2021) 1981–1993.

[32] Z. Zhao, D. Xu, S. Li, et al., Activation of liver X receptor attenuates oleic acid-induced acute respiratory distress syndrome, Am. J. Pathol. 186 (10) (2016) 2614–2622.

[33] M. El-Shabrawy, M.E. Alsadik, M. El-Shafei, et al., Interleukin-6 and C-reactive protein/albumin ratio as predictors of COVID-19 severity and mortality, Egypt. J. Bronchol. 15 (1) (2021) 5, https://doi.org/10.1186/s43168-021-00054-1.

[34] R. Rasool, I. Ashiq, I.A. Shera, Q. Yousuf, Z.A. Shah, Study of serum interleukin (IL) 18 and IL-6 levels in relation with the clinical disease severity in chronic idiopathic urticaria patients of Kashmir (North India), Asia Pac. Allergy 4 (4) (2014) 206–211, https://doi.org/10.5415/apallergy.2014.4.4.206.

[35] A.E. Muruato, C.R. Fontes-Garfias, P. Ren, et al., A High-throughput Neutralizing Antibody Assay for COVID-19 Diagnosis and Vaccine Evaluation, Preprint. bioRxiv, 2020, https://doi.org/10.1101/2020.05.21.109546, 2020.05.21.109546. Published 2020 May 22.

[36] N.V. Goncharov, D.A. Belinskaia, V.I. Shmurak, M.A. Terpilowski, R.O. Jenkins, P. V. Avdonin, Serum albumin binding and esterase activity: mechanistic interactions with organophosphates, Molecules 22 (7) (2017 Jul 18) 1201.

[37] O.A. Roveri, S.E. Braslavsky, π-Cation interactions as the origin of the weak absorption at 532 nm observed in tryptophan-containing polypeptides, Photochem. Photobiol. Sci. 11 (6) (2012) 962–966.

[38] Maxim A. Lutoshkin, Boris N. Kuznetsov, Vladimir A. Levdansky, Spectrophotometric and quantum-chemical study of acid-base and complexing properties of (±)-taxifolin in aqueous solution, Heterocycl. Commun. 23 (5) (2017).

[39] N.A.N. Hanafy, A. Quarta, R. Di Corato, L. Dini, C. Nobile, V. Tasco, S. Carallo, M. Cascione, A. Malfettone, J. Soukupova, R. Rinaldi, I. Fabregat, S. Leporatti, Hybrid polymeric-protein nano-carriers (HPPNC) for targeted delivery of TGFβ inhibitors to hepatocellular carcinoma cells, J. Mater. Sci. Mater. Med. 28 (8) (2017 Aug) 120.

[40] N.A.N. Hanafy, S. Leporatti, M. El-Kemary, Mucoadhesive curcumin crosslinked carboxy methyl cellulose might increase inhibitory efficiency for liver cancer treatment, Mater. Sci. Eng. C Mater. Biol. Appl. 116 (2020), 111119.

[41] N.J. Prat, A.D. Meyer, T. Langer, R.K. Montgomery, B.K. Parida, A.I. Batchinsky, A. P. Cap, Low-dose heparin anticoagulation during extracorporeal life support for acute respiratory distress syndrome in conscious sheep, Shock 44 (6) (2015 Dec) 560–568.

[42] C.F. Gonçalves-de-Albuquerque, A.R. Silva, P. Burth, et al., Oleic acid induces lung injury in mice through activation of the ERK pathway, Mediat. Inflamm. 2012 (2012) 11.

[43] G.H. Crocker, J.H. Jones, Effects of oleic acid-induced lung injury on oxygen transport and aerobic capacity, Respir. Physiol. Neurobiol. 1 (196) (2014 Jun) 43–49.

[44] A. Haque, A.H. Scultetus, F. Arnaud, et al., The emulsified PFC Oxycyte® improved oxygen content and lung injury score in a swine model of oleic acid lung injury (OALI), Lung 194 (2016) 945–957.

[45] B.F. Dickey, R.S. Thrall, J.R. McCormick, P.A. Ward, Oleic-acid-induced lung injury in the rat. Failure of indomethacin treatment or complement depletion to ablate lung injury, Am. J. Pathol. 103 (3) (1981 Jun) 376–383.

[46] C. Harris, H. Demmelmair, A. von Berg, et al., Associations between fatty acids and low-grade inflammation in children from the LISAplus birth cohort study, Eur. J. Clin. Nutr. 71 (2017) 1303–1311.

[47] K.R. Bewley, N.S. Coombes, L. Gagnon, et al., Quantification of SARS-CoV-2 neutralizing antibody by wild-type plaque reduction neutralization, microneutralization and pseudotyped virus neutralization assays, Nat. Protoc. 16 (2021) 3114–3140, https://doi.org/10.1038/s41596-021-00536-y.

[48] N. Islam, V. Ferro, Recent advances in chitosan-based nanoparticulate pulmonary drug delivery, Nanoscale 8 (2016) 14341.

[49] C.F. Gonçalves-de-Albuquerque, A.R. Silva, P. Burth, M.V. Castro-Faria, H. C. Castro-Faria-Neto, Acute respiratory distress syndrome: role of oleic acid-triggered lung injury and inflammation, Mediat. Inflamm. 2015 (2015), 260465.

[50] L. Nieuwenhuizen, P.G. De Groot, J.C. Grutters, D.H. Biesma, A review of pulmonary coagulopathy in acute lung injury, acute respiratory distress syndrome and pneumonia, Eur. J. Haematol. 82 (6) (2009) 413–425.

[51] A. Aguilar-Lemarroy, A. López-Uribe, J. Sánchez-Corona, L.F. Jave-Suárez, Severe acute respiratory syndrome coronavirus 2 ORF3a induces the expression of ACE2 in oral and pulmonary epithelial cells and the food supplement Vita Deyun® diminishes this effect, Exp. Ther. Med. 21 (5) (2021 May) 485, https://doi.org/10.3892/etm.2021.9916. Epub 2021 Mar 16. PMID: 33790994; PMCID: PMC8005676.

[52] M.L. De Pellegrin, A. Rohrhofer, P. Schuster, B. Schmidt, P. Peterburs, A. Gessner, The potential of herbal extracts to inhibit SARS-CoV-2: a pilot study, Clin. Phytosci. 7 (1) (2021) 29, https://doi.org/10.1186/s40816-021-00264-6.

[53] M. Villena-Tejada, I. Vera-Ferchau, A. Cardona-Rivero, R. Zamalloa-Cornejo, M. Quispe-Florez, Z. Frisancho-Triveño, et al., Use of medicinal plants for COVID-19 prevention and respiratory symptom treatment during the pandemic in Cusco, Peru: a cross-sectional survey, PLoS ONE 16 (9) (2021), e0257165.

[54] F. Zhao, D. Shi, T. Li, L. Li, M. Zhao, Silymarin attenuates paraquat-induced lung injury via Nrf2-mediated pathway in vivo, Clin. Exp. Pharmacol. Physiol. 42 (2015) 988–998, https://doi.org/10.1111/1440-1681.12448.

[55] M. Wang, R. Cao, L. Zhang, X. Yang, J. Liu, M. Xu, et al., Remdesivir and chloroquine effectively inhibit the recently emerged novel coronavirus (2019-nCoV) in vitro, Cell Res. 1 (2020) 3.

[56] M. Kandeel, M. Al-Nazawi, Virtual screening and repurposing of FDA approved drugs against COVID-19 main protease, Life Sci. 15 (2020) 251.

[57] D.P.P. Shanmugarajan, B.R.P. Kumar, B. Suresh, Curcumin to inhibit binding of spike glycoprotein to ACE2 receptors: computational modelling, simulations, and ADMET studies to explore curcuminoids against novel SARS-CoV-2 targets, RSC Adv. 10 (2020) 31385–31399.

[58] A. Goc, W. Sumera, M. Rath, A. Niedzwiecki, Phenolic compounds disrupt spike-mediated receptor-binding and entry of SARS-CoV-2 pseudo-virions, PLoS One 16 (6) (2021 Jun 17), e0253489.

[59] N.A.N. Hanafy, A. Quarta, R. Di Corato, L. Dini, C. Nobile, V. Tasco, S. Carallo, M. Cascione, A. Malfettone, J. Soukupova, R. Rinaldi, I. Fabregat, S. Leporatti, Hybrid polymeric-protein nano-carriers (HPPNC) for targeted delivery of TGFβ inhibitors to hepatocellular carcinoma cells, J. Mater. Sci. Mater. Med. 28 (8) (2017 Aug) 120.

[60] Hanafy NAN, A. Quarta, M.M. Ferraro, L. Dini, C. Nobile, M.L. De Giorgi, S. Carallo, C. Citti, A. Gaballo, G. Cannazza, R. Rinaldi, G. Giannelli, S. Leporatti, Polymeric nano-micelles as novel cargo-carriers for LY2157299 liver cancer cells delivery, Int. J. Mol. Sci. 19 (3) (2018 Mar 6).

[61] N.A. Hanafy, M.M. Ferraro, A. Gaballo, L. Dini, V. Tasco, C. Nobile, M.L. De Giorgi, S. Carallo, R. Rinaldi, S. Leporatti, Fabrication and characterization of ALK1fc-loaded fluoro-magnetic nanoparticles rods for inhibiting TGF β1 in HCC, RSC Adv. 6 (2016) 48834–48842.

[62] N.A.N. Hanafy, S. Leporatti, M. El-Kemary, Mucoadhesive hydrogel nanoparticles as smart biomedical drug delivery system, Appl. Sci. 9 (5) (2019) 825.